Biosensors and Bioelectronics 45 (2013) 6–12

Contents lists available at SciVerse ScienceDirect

Biosensors and Bioelectronics

journal homepage: www.elsevier.com/locate/bios

A CMOS magnetic microbead-based capacitive biosensor array with on-chip electromagnetic manipulation

An-Yu Chang [b], Michael S.-C. Lu [a,b,c,*]

[a] Department of Electrical Engineering, National Tsing Hua University, Hsinchu 30013, Taiwan, ROC
[b] Institute of Electronics Engineering, National Tsing Hua University, Hsinchu 30013, Taiwan, ROC
[c] Institute of NanoEngineering and Microsystems, National Tsing Hua University, Hsinchu 30013, Taiwan, ROC

ARTICLE INFO

Article history:
Received 10 November 2012
Received in revised form
6 January 2013
Accepted 16 January 2013
Available online 29 January 2013

Keywords:
Capacitive biosensor
CMOS
Magnetic microbead
Microcoil

ABSTRACT

Magnetic microbeads are widely used in biotechnology and biomedical research for manipulation and detection of cells and biomolecules. Most lab-on-chip systems capable of performing manipulation and detection require external instruments to perform one of the functions, leading to increased size and cost. This work aims at developing an integrated platform to perform these two functions by implementing electromagnetic microcoils and capacitive biosensors on a CMOS (complementary metal oxide semiconductor) chip. Compared to most magnetic-type sensors, our detection method requires no externally applied magnetic fields and the associated fabrication is less complicated. In our experiment, microbeads coated with streptavidin were driven to the sensors in the center of microcoils with functionalized anti-streptavidin antibody. Detection of a single microbead was successfully demonstrated using a capacitance-to-frequency readout. The average capacitance changes for the experimental and control groups were −5.3 fF and −0.2 fF, respectively.

1. Introduction

With the advances in micro-system technologies, lab-on-chips have become a major research area for miniaturizing biological assays towards point-of-care diagnostics. An ideal lab-on-chip is desired to be capable of manipulating and sensing biological samples. With these dual functions, various samples can be sorted and detected with a shortened response time and sensitivity can be enhanced by pre-concentration of diluted samples. In many applications, microparticles functionalized with target biomolecules are used for convenient manipulation and detection; for example, magnetic microbeads (Gijs, 2004) have been utilized extensively in biomolecule separation and purification, immunoassays, magnetic resonance imaging, and hyperthermia. They can be conveniently manipulated by using permanent magnets or electromagnets. As compared to fluorescent labeling for biosensing, magnetic microbeads are relatively stable over time because the magnetism is not affected by reagent chemistry or subject to photo-bleaching.

Detection of magnetic labels can be utilized in biosensing applications for DNA arrays (Edelstein et al., 2000; Schotter et al., 2004; Graham et al., 2005; Xu et al., 2008), immunoassays (Meyer et al., 2007; Wirix-Speetjens et al., 2007; Dittmer et al., 2008; Mujika et al., 2009; Mak et al., 2010), and functional bioassays (Janssen et al., 2008). Detection methods include superconducting quantum interference device (SQUID) (Chemla et al., 2000; Itozaki, 2003; Carr et al., 2007; Raphael et al., 2010), magnetoresistive sensors (Lagae et al., 2002; Schotter et al., 2004; Graham et al., 2005; Megens, Prins, 2005; de Boer et al., 2007; Dittmer et al., 2008; Janssen et al., 2008; Mujika et al., 2009; Mak et al., 2010; Xu et al., 2008), nuclear magnetic resonance (Sun et al., 2009; Kaittanis et al., 2011), Hall sensors (Togawa et al., 2005; Aytur et al., 2006), inductive coils (Richardson et al., 2001; Baglio et al., 2005; Wang et al., 2009), and optical sensors (Lehmann et al., 2008). For example, Edelstein et al. (2000) developed a microsystem for capture and detection of magnetic microbeads on a chip containing an array of giant-magnetoresistive sensors. Magnetic fields were applied for sensing and also removing any beads that are not specifically bound to the surface. Most of the magnetic-type sensors require externally generated magnetic fields for detection since those microbeads are inherently superparamagnetic. Wang et al. (2009) reported detection of a single magnetic microbead without a magnetic biasing field by using a frequency-shift oscillator whose inductance was varied by bounded magnetic beads.

Manipulation and detection of magnetic microparticles (Smistrup et al., 2005; Yang et al., 2008) have been demonstrated by many lab-on-chips. Most of them rely on external means to perform one of the functions, leading to increased size,

* Corresponding author at: National Tsing Hua University, Department of Electrical Engineering, 101 Sec. 2 Kuang-Fu Rd., Hsinchu , Taiwan.
Tel.: +1 886 3 516 2220; fax: +1 886 3 575 2120.
E-mail address: sclu@ee.nthu.edu.tw (M.-C. Lu).

0956-5663/$ - see front matter © 2013 Elsevier B.V. All rights reserved.
http://dx.doi.org/10.1016/j.bios.2013.01.033

complexity, and cost of the overall system. A miniaturized system can be implemented by on-chip integration of these capabilities. Several works (Edelstein et al., 2000; Lagae et al., 2002; Janssen et al., 2008) reported integrated chips consisting of current-carrying wires to manipulate and magnetize microbeads and magnetoresistive sensors for microbead detection. For implementation of a large array, it is often desirable to use an integrated-circuit process to facilitate signal routing, multiplexing, and processing. Lehmann et al. (2008) reported a CMOS chip comprising micro-coils for magnetic manipulation and single photon avalanche diodes for optical detection of fluorescently labeled magnetic beads. In addition to magnetic microbeads, manipulation and detection of dielectric microbeads can also be realized on the same chip by combining electrokinetic actuation with optical sensors (Manaresi et al., 2003), ion-sensitive field-effect transistor) (ISFET) sensors (Castellarnau et al., 2007) and impedimetric sensors (Park et al., 2010; Chuang et al., 2011).

Compared to most of the aforementioned magnetic sensing techniques, capacitive sensing does not require additional deposition of magnetic thin films and application of magnetic fields for detection. A typical magnetic microbead consists of iron oxide nanoparticles surrounded by a polymer coating with functionalized biomolecules for selective binding. A capacitance change due to a dielectric property change and/or carried electric charges is induced when a magnetic microbead binds to electrically biased electrodes. Most of the capacitive biosensors (Loyprasert et al., 2008; de Vasconcelos et al., 2009; Qureshi et al., 2010) are not implemented in an integrated-circuit process (e.g. CMOS). Capacitive biosensors fabricated in a CMOS process (Stagni et al., 2007; Prakash and Abshire, 2007; Grafar-Zadeh et al., 2008; Lu et al., 2010) can provide enhanced signal-to-noise ratio by minimizing the effect of parasitic capacitances observed at the sensing node. To date, capacitive detection of a single magnetic microbead has not been demonstrated by a CMOS biochip.

Toward this end, this work presents a CMOS capacitive sensor array with integrated microcoils for magnetic manipulation. The array size can be conveniently scaled up to provide detection of multiple samples and large amount of data for statistical analysis. The active manipulation capability effectively enhances the probability of capturing a single magnetic microbead for the ensuing detection. Each microcoil can attract a microbead to its center where a capacitive sensor is located. The capacitance change leads to an output frequency change of the oscillator-based sensing circuit. Detection of a single microbead functionalized with streptavidin is successfully demonstrated. More details regarding to the design and measurement of the CMOS chip are presented in the following sections.

2. Materials and methods

2.1. Materials

3-Aminopropyltriethoxysilane (APTES), ethanolamine, and anti-streptavidin antibody were purchased from Sigma-Aldrich (USA). Glutaraldehyde in aqueous solution (25%) and magnetic microbeads coated with streptavidin (diameter = 10 μm; binding capacity for FITC-biotin > 1000 pmol/mg; activity streptavidin POD > 1000 U/g) were purchased from Fluka (USA). Phosphate buffer solution (PBS) was prepared in deionized (DI) water (pH = 7; resistivity = 18.2 MΩ cm).

2.2. Operating principle

The operating principle of magnetic microbead-based manipulation and capacitive detection is illustrated in Fig. 1. A two-polysilicon-four-metal (2P4M) 0.35-μm CMOS process is utilized

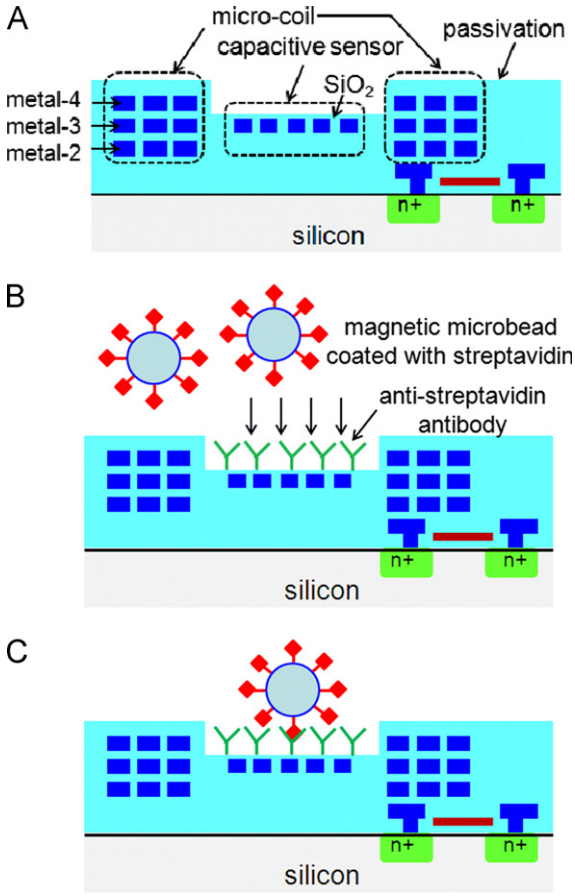

Fig. 1. Operating principle of magnetic microbead-based manipulation and capacitive detection: (A) cross-sectional view of the fabricated CMOS chip; (B) magnetic actuation of streptavidin-coated magnetic microbeads toward the capacitive sensor with functionalized anti-streptavidin antibody; (C) capacitive detection of the remaining microbead after specific binding.

for fabrication of the 8 × 8 micro-manipulation and sensor array. As shown by the cross-sectional view in Fig. 1A, each basic element in the array consists of a microcoil for electromagnetic actuation and a set of interdigitated microelectrodes in its center for capacitive detection. The microcoil is constructed using multiple metal layers provided by the CMOS process in order to increase the number of turns and thus the produced electromagnetic force. The passivation thin films (1 μm Si_3N_4 and 0.45 μm SiO_2) for chip protection are kept on top of microcoils but removed in the electrode areas by foundry's dry etching process. The thin intermetal silicon dioxide (~0.3 μm) remaining on electrode surface is used for immobilizing bio-recognition elements, such as anti-streptavidin antibody used in this work. As shown in Fig. 1B, magnetic microbeads functionalized with streptavidin are electromagnetically moved toward the sensor in the microcoil center. The electrode is slightly larger than a microbead, thereby allowing only one microbead to remain on its surface for specific binding and the following capacitive detection (Fig. 1C). The magnetic microbead used in this study is a polymer (polystyrene) microsphere containing a large number of nanomagnets made of iron oxide. The capacitance change near the bead-electrode interface is attributed to a dielectric property change and/or electric charges.

2.3. Surface functionalization and immobilization

CMOS chips were firstly washed by ethanol and acetone solutions for 10 min respectively to remove contaminants and

introduce –OH on the oxide surface. Then the chips were immersed in 2% APTES ethanol solution for 30 min to introduce amino groups on the oxide surface. The chips were then washed with ethanol (99.5%) for three times to remove unbound APTES. In the following step, the chips were immersed in 2.5% glutaraldehyde solution prepared from 10 mM PBS (pH=7.0) for 2 h followed by PBS wash. Finally, 10 μM anti-streptavidin antibodies were coupled to the sensor surface in PBS for 10 h. The un-reacted aldehyde groups were blocked by mixing with 50 mM ethanolamine for 1 h followed by PBS wash.

Solution containing magnetic microbeads functionalized with streptavidin was diluted by 10 mM PBS for test of selective binding following the aforementioned steps. For the experimental group, many microbeads were observed to remain on oxide surface functionalized with anti-streptavidin antibody after wash, as shown in Fig. S1A. For the control group without functionalized anti-streptavidin antibody, there was nearly no remaining microbeads as shown in Fig. S1B.

2.4. Microcoil and capacitive sensor array

Implementation of a large and scalable manipulation and biosensor array in a CMOS process is facilitated by the on-chip powerful electronics for signal processing and multiplexing. As shown by the schematic in Fig. 2A, the chip design comprises 8×8 microcoils and the center of each microcoil contains a capacitive sensor. Two microcoil designs are implemented, one (type A) with a narrower linewidth (1 μm) but more turns and the other (type B) with a wider linewidth (10 μm) and less turns. Multiple CMOS metallization layers are used to form 25 turns and 20 turns for the type-A and type-B microcoils whose resistances are 350 and 40 Ω, respectively. There are four rows of type-A and type-B microcoils respectively on the chip. As illustrated in Fig. 2A, electromagnetic driving of each microcoil is controlled by column/row decoders. The current flowing through each microcoil is provided by a current-mirror circuit whose current value is adjustable up to 30 mA through a three-bit decoder control. It is desired to produce a magnetic force in the order of tens of picoNewtons for driving magnetic microbeads. Fig. 2B shows the finite-element simulation (Ansoft Maxwell) of the magnetic field distribution for the type-B microcoil driven at 10 mA. The maximum magnetic field intensity occurs in the center and the produced magnetic force is 90pN. The force produced by the type-A microcoil under the same current is 92pN.

The interdigitated microelectrodes used for capacitive detection contain five pairs of 10-μm long electrodes separated by a gap of 0.5 μm. The electrode size is designed slightly larger than the magnetic microbead in order to demonstrate single-bead detection. Electric field lines across a smaller electrode gap are more effectively affected by an attached magnetic microbead to increase the capacitance change. The choice of 0.5 μm is the minimum value allowed by the foundry's design rules. Schematic of the CMOS oscillator readout is depicted in Fig. 2C. The comparator in the circuit triggers the charging and discharging of the capacitor (C_s) at a switching level V_{SW} and results in a pulse stream whose frequency (f) varies with C_s as represented by

$$f = \left[\frac{C_s V_{sw}}{I_B} + \tau_d\right]^{-1} \quad (1)$$

where I_B is the bias current and τ_d is the time delay caused by the comparator and the inverter delay stage. The output frequency is inversely proportional to the capacitance C_s with a negligible τ_d. The capacitor C_s comprises the interdigitated microelectrode, represented by C_{elec}, in parallel with the parasitic and circuit input capacitances, represented by C_p, and the bead-electrode interface capacitance C_{bead}. Since the capacitances C_{elec} and C_p are positively charged by the current source, more positive or negative charges at the bead-electrode interface form an effective positive or negative capacitance that increases and decreases the

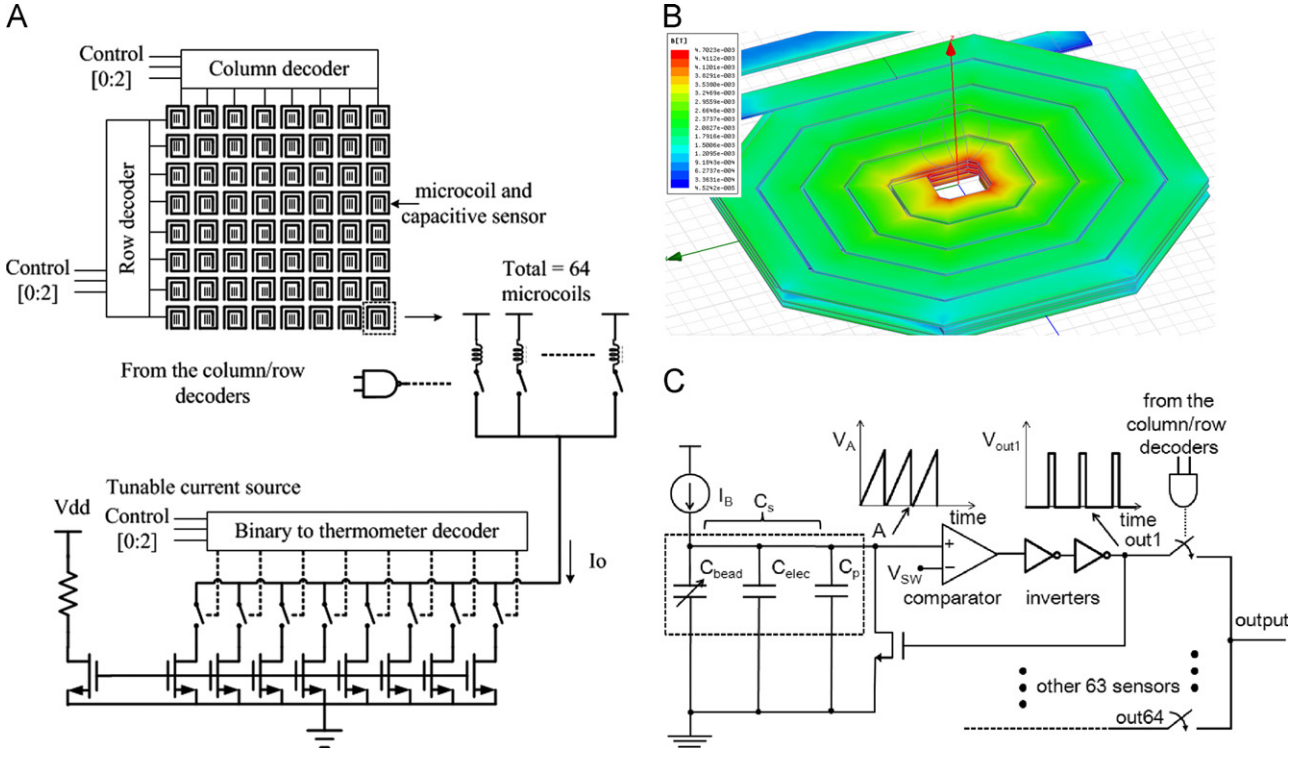

Fig. 2. (A) Schematic of the CMOS micro-manipulation and biosensing array. The tunable current source for driving microcoils is also illustrated. (B) Finite-element simulation of magnetic fields of the type-B microcoil and (C) Schematic of the capacitive sensing circuit.

total capacitance C_s. The value of C_{elec} is analyzed by finite-element simulation (CoventorWare, Coventor Inc.) to be 7 fF. Compared to non-integrated capacitive sensors, capacitive sensitivity is significantly enhanced by monolithic integration to minimize the capacitance C_p. As depicted in Fig. 2C, when the ramp signal V_A produced by the charged capacitor C_s reaches the switching level of the comparator, the reset transistor is turned on to discharge the capacitor to ground potential. Digital output pulses are automatically sustained by the feedback loop. Each output in the 8×8 sensor array is sequentially measured by control of the column/row decoders.

3. Experiment

Fig. 3 shows the micrograph of the CMOS chip and the scanning electron micrograph of a type-B microcoil with a capacitive sensor in the center. Data collection and timing control of the CMOS digital circuits were achieved through a data acquisition card (NI USB-6008) and the LabVIEW software installed in a computer. Output waveforms were monitored on a digital oscilloscope (Agilent DSOX 3014A) and pulse frequencies were recorded and transmitted through a NI GPIB-USB-HS cable (which includes a GPIB controller and a USB connector) to the computer. Fig. S2 shows one of the waveforms measured in air. Pulse frequencies of the 4×8 sensors surrounded by the type-A microcoils were measured to be 5.245 ± 0.435 MHz in air, and those of the ones surrounded the type-B microcoils were 4.06 ± 0.33 MHz. Since the measured capacitance values were inversely proportional to the output frequencies, the capacitances C_s for the two cases were calculated to be 23.3 ± 1.9 fF and 30.1 ± 2.4 fF, respectively, for $I_B = 200$ nA and $V_{SW} = 1.65$ V. The difference is owing to that the routing wire with respect to the type-B microcoil produces a larger parasitic capacitance. Based on a simulated electrode capacitance C_{elec} of 7 fF, the capacitances C_p for the two cases are about 16 and 23 fF, respectively.

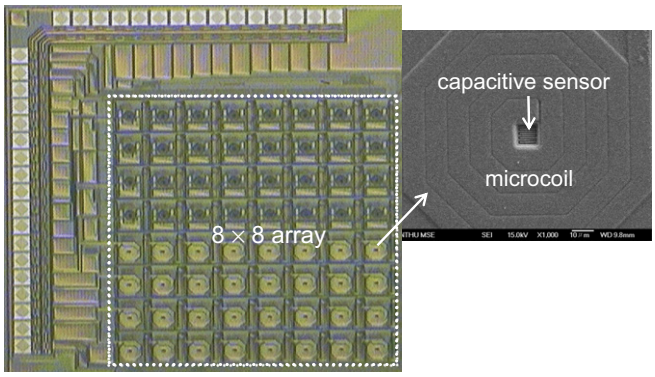

Fig. 3. Micrograph of the CMOS chip and scanning electron micrograph of one of the type-B microcoils containing a capacitive sensor.

Sensor outputs were then measured during the surface modification and functionalization steps after adding APTES, glutaraldehyde, anti-streptavidin antibody, and ethanolamine. Each sensor was recorded for one second, so it took 64 s to complete one measurement of the 8×8 array. Fig. 4A–D show the measured percentage capacitance changes, with respect to time, of three typical sensors during these steps. The capacitance increase associated with APTES in Fig. 4A could be owing to that the amino group ($pK_a > 9$) was protonated to $-NH_3^+$ to result in more positive charges. The capacitance change associated with the electrically neutral glutaraldehyde in Fig. 4B varied within $\pm 5\%$ of the nominal values. In Fig. 4C, the capacitance increased by less than 10% after adding anti-streptavidin antibody, which could be attributed to a change of dielectric property and/or electric charges at the interface. The capacitance decrease in Fig. 4D could

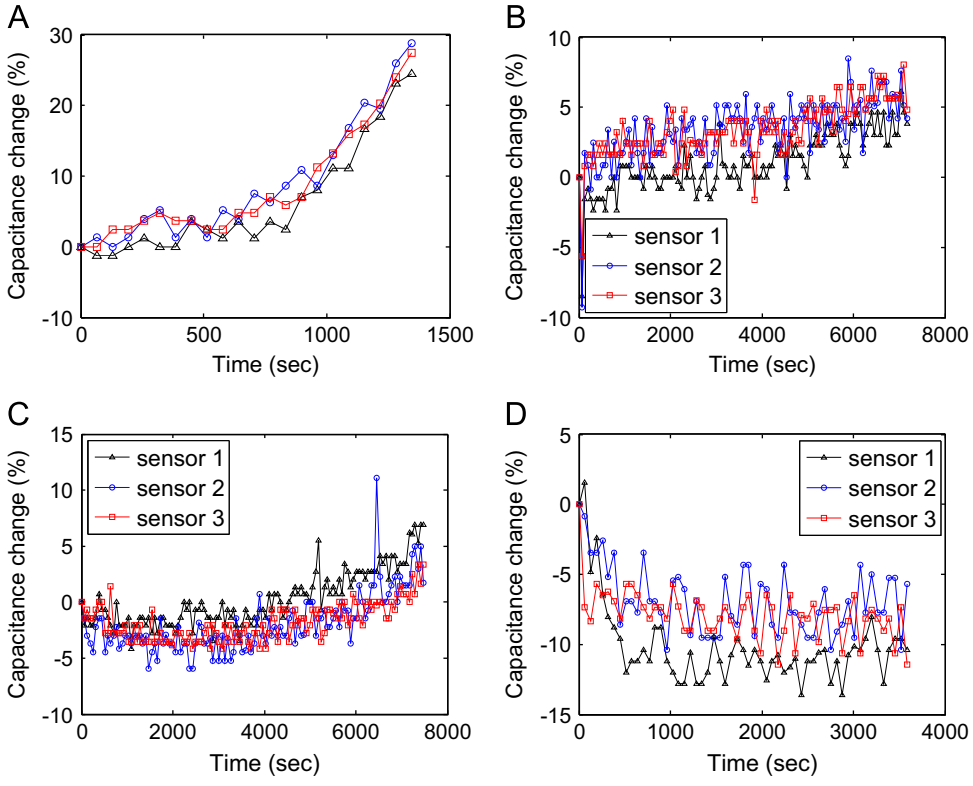

Fig. 4. Measured percentage capacitance changes from three of the capacitive sensors after adding (A) APTES, (B) glutaraldehyde, (C) anti-streptavidin antibody and (D) ethanolamine.

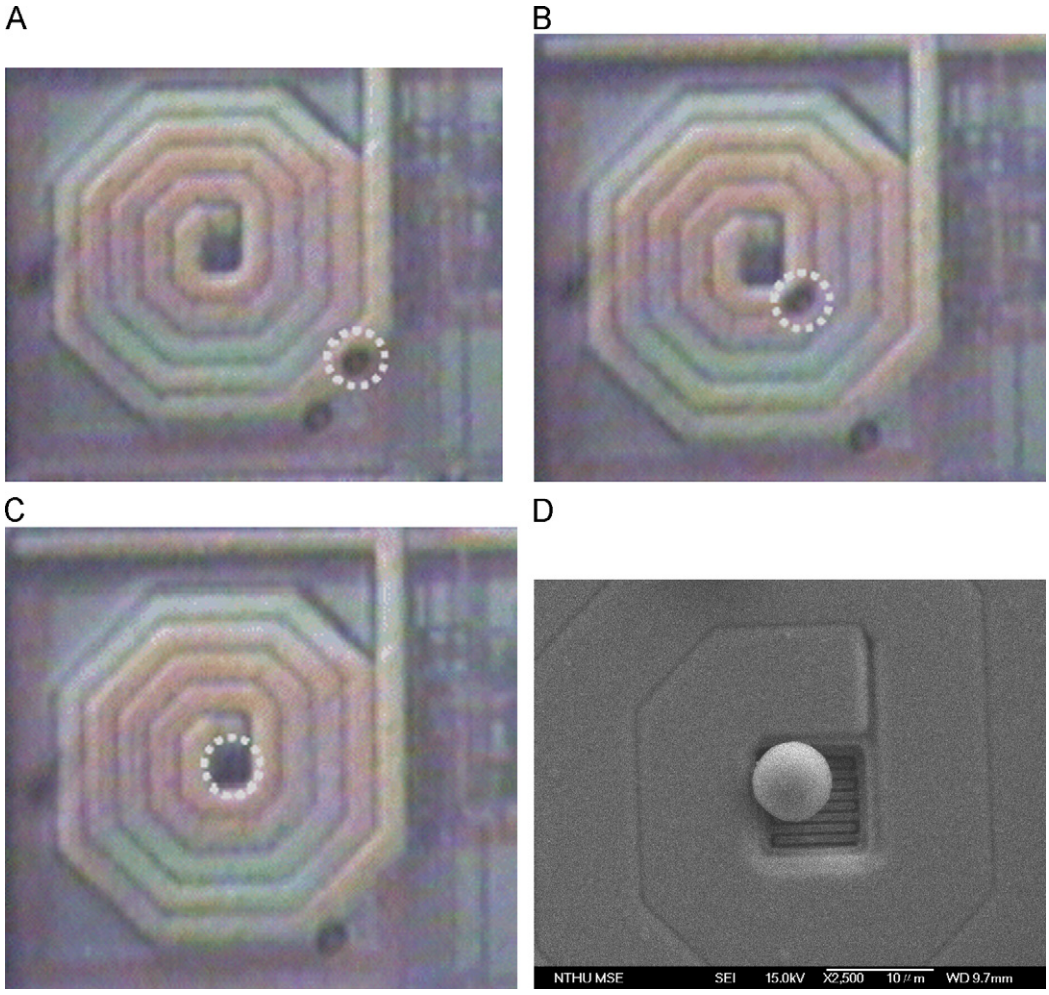

Fig. 5. (A)–(C): electromagnetic actuation of a magnetic microbead to the center of a type-B microcoil; (D) scanning electron micrograph of a type-B microcoil with a captured microbead after specific binding.

be due to the produced negative charges, since COOH and NH_3^+ of anti-streptavidin antibody could be converted to COO– and NH_2 respectively due to an increased pH by adding 50 mM ethanolamine.

In the next step, solution containing streptavidin-coated magnetic microbeads was diluted by 10 mM PBS and added to the chip by a micropipette. The microcoils were turned on in advance so the beads were driven before they landed on surface; otherwise more driving current was required to overcome surface adhesion force. To save power consumption, each row of microcoils was turned on sequentially for 1/8 s in a repeated manner. It was found that the type-A and type-B microcoils required about 10 mA and 25 mA respectively to move microbeads to their center. Fig. 5A–C show that a microbead was gradually moved from the outer edge of a type-B microcoil to it center. After specific binding of streptavidin and anti-streptavidin antibody on sensor surface, the chip was washed and dried in air. Fig. 5D shows the scanning electron micrograph of a type-B microcoil with a captured microbead.

Fifteen sensors of the array showed a captured microbead. Fig. 6A show the result of one of these sensors, and more results are illustrated in Fig. S3A and B. The two curves in the figure represent the measurements where the chip was placed in air to dry after adding ethanolamine (i.e., before adding microbeads) and manipulation of microbeads, respectively. Both output frequencies gradually increased due to a decreased interface capacitance resulting from a gradually reduced dielectric constant while dried in air. The final frequency for the sensor with a captured microbead was higher than the other curve, indicating a decrease in the overall capacitance C_s. For the sensors without a captured microbead (control group), the measured final frequencies of the two curves as shown in Fig. 6B were almost the same as expected. More similar results are illustrated in Fig. S3C and D.

The decreased bead-electrode interface capacitance due to a captured microbead could be attributed to the produced negative changes produced from two sources: (1) streptavidin coated on microbeads carries negative charges in the solution (pH ≈ 7) due to its isoelectric point (~ 5); (2) the charging and discharging waveform (0–1.65 V) on sensing electrodes produces a positive root-mean-square dc voltage that polarizes the microbead polymer to generate negative charges near the bead-electrode interface. The smallest and largest capacitance changes of the 15 sensors with a captured microbead were -2.1 fF and -10.2 fF, respectively. The average capacitance change was -5.3 fF with a standard deviation of 2.5 fF. The other sensors without a microbead showed much less capacitance changes ranging between -1.9 fF and 1.2 fF, with an average of -0.2 fF and a standard deviation of 0.7 fF.

4. Discussion and conclusion

This work presents the first attempt to integrate microcoils and capacitive sensors to implement a monolithic micro-manipulation

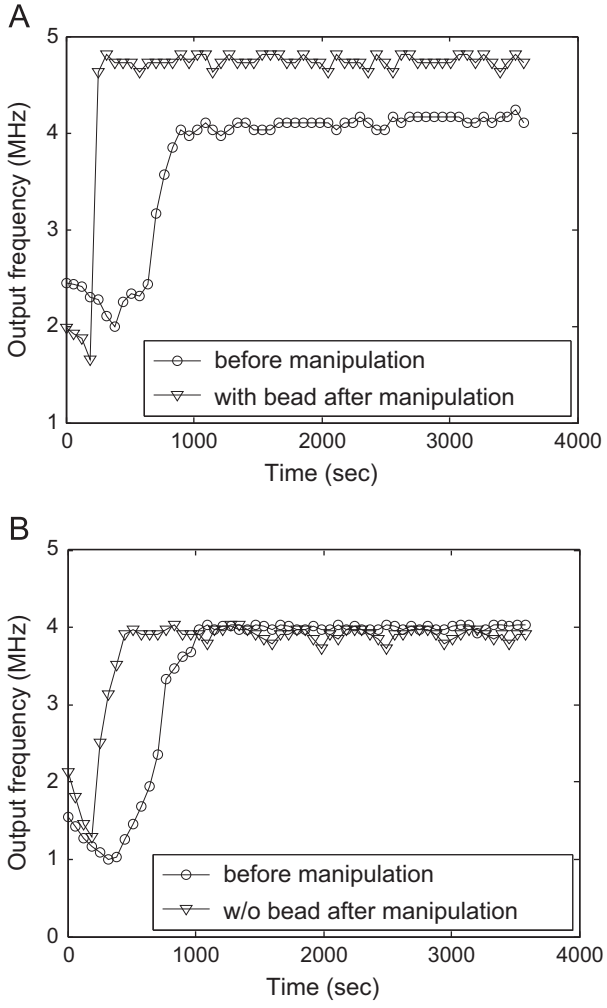

Fig. 6. Measured output frequencies of capacitive sensors before and after magnetic manipulation: (A) one of the sensors with a captured microbead and (B) one of the sensors without a microbead.

and biosensing array. Magnetic microbeads are moved to the desired sensor locations by on-chip magnetic actuation without requiring an external magnet. Single-microbead detection is successfully demonstrated by capacitive sensors with a similar size of a microbead. The associated capacitance change is quite small in the femto-farad range, which justifies the need for monolithic sensor integration to enhance capacitive sensitivity. The technology presented in this work is especially useful for building large DNA arrays and immunoassays to provide detection of multiple samples and large amount of data for statistical analysis. Without on-chip circuitry, the number of fabricated sensing devices is commonly limited by the difficulty to complete signal routing, whereas the issue of scalability does not exist for our work. In addition, as compared to other CMOS magnetic sensors, our capacitive sensors require no additional deposition of magnetic thin films and application of magnetic fields for detection. The measured result demonstrates that the average capacitance changes for the experimental and control groups are -5.3 fF and -0.2 fF, respectively, showing a ratio of more than an order of magnitude. It is reasonable to assume that the detectable capacitance change varies linearly with the microbead size. Therefore our sensor array should still be able to detect a microbead of 1 μm in diameter. For more sensitive detection of a micron-sized magnetic microbead in the future, it is better to use a smaller sensing electrode to provide a better match in size and a higher percentage capacitance change than the electrode used in this work. In addition to magnetic microbeads, dielectric microbeads with coated biomolecules can also be utilized as the vehicle for micro-manipulation and detection. It would be interesting to compare the effectiveness and performance of the biochips implemented for these two types of microbeads.

Acknowledgment

The authors would like to thank the National Tsing Hua University and the National Science Council, Taiwan R.O.C., for their funding support, the National Chip Implementation Center for chip fabrication, and the National Center for High-Performance Computing for support of simulation software. We also thank Prof. Yuh-Shyong Yang and Dr. Chih-Heng Lin for their valuable suggestions.

Appendix A. Supporting information

Supplementary data associated with this article can be found in the online version at http://dx.doi.org/10.1016/j.bios.2013.01.033.

References

Aytur, T., Foley, J., Anwar, M., Boser, B., Harris, E., Beatty, P.R., 2006. Journal of Immunological Methods 314, 21–29.
Baglio, S., Castorina, S., Savalli, N., 2005. IEEE Sensors Journal 5, 372–384.
Carr, C., Matlachov, A.N., Sandin, H., Espy, M.A., Kraus, R.H., 2007. IEEE Transactions on Applied Superconductivity 17, 808–811.
Castellarnau, M., Zine, M., Bausells, J., Madrid, C., Juárez, A., Samitier, J., Errachid, A., 2007. Sensors and Actuators B (Chemical) 120, 615–620.
Chemla, Y.R., Grossman, H.L., Poon, Y., McDermott, R., Stevens, R., Alper, M.D., Clarke, J., 2000. Proceedings of the National Academy of Sciences 97, 14268–14272.
Chuang, C.H., Huang, Y.W., Wu, Y.T., 2011. Sensors 11, 11021–11035.
de Boer, B.M., Kahlman, J.A.H.M., Jansen, T.P.G.H., Duric, H., Veen, J., 2007. Biosensors and Bioelectronics 22, 2366–2370.
de Vasconcelos, E.A., Peres, N.G., Pereira, C.O., da Silva, V.L., da Silva Jr., E.F., Dutra, R.F., 2009. Biosensors and Bioelectronics 25, 870–876.
Dittmer, W.U., de Kievit, P., Prins, M.W.J., Vissers, J.L.M., Mersch, M.E.C., Martens, M.F.W.C., 2008. Journal of Immunological Methods 338, 40–46.
Edelstein, R.L., Tamanaha, C.R., Sheehan, P.E., Miller, M.M., Baselt, D.R., Whitman, L.J., Colton, R.J., 2000. Biosensors and Bioelectronics 14, 805–813.
Gijs, M.A.M., 2004. Microfluidics and Nanofluidics 1, 22–40.
Ghafar-Zadeh, E., Sawan, M., Therriault, D., 2008. Sensors and Actuators A 141, 454–462.
Graham, D.L., Ferreira, H.A., Feliciano, N., Freitas, P.P., Clarke, L.A., Amaral, M.D., 2005. Sensors and Actuators B (Chemical) 107, 936–944.
Itozaki, H., 2003. Superconductor Science and Technology 12, 1340.
Janssen, X.J.A., van IJzendoorn, L.J., Prins, M.W.J., 2008. Biosensors and Bioelectronics 23, 833–838.
Kaittanis, C., Banerjee, T., Santra, S., Santiesteban, O.J., Teter, K., Perez, J.M., 2011. Bioconjugate Chemistry 22, 307–314.
Lagae, L., Wirix-Speetjens, R., Das, J., Graham, D., Ferreira, H., Freitas, P.P.F., Borghs, G., De Boeck, J., 2002. Journal of Applied Physics 91, 7445–7447.
Lehmann, U., Sergio, M., Pietrocola, S., Dupont, E., Niclass, C., Gijs, M.A.M., Charbon, E., 2008. Sensors and Actuators. B (Chemical) 132, 411–417.
Loyprasert, S., Thavarungkul, P., Asawatreratanakul, P., Wongkittisuksa, B., Limsakul, C., Kanatharana, P., 2008. Biosensors and Bioelectronics 24, 78–86.
Lu, M.S.-C., Chen, Y.C., Huang, P.C., 2010. Biosensors and Bioelectronics 26, 1093–1097.
Mak, A.C., Osterfeld, S.J., Yu, H., Wang, S.X., Davis, R.W., Jejelowo, O.A., Pourmand, N., 2010. Biosensors and Bioelectronics 25, 1635–1639.
Manaresi, N., Romani, A., Medoro, G., Altomare, L., Leonardi, A., Tartagni, M., Guerrieri, R., 2003. IEEE Journal of Solid-State Circuits 38, 2297–2305.
Megens, M., Prins, M., 2005. Journal of Magnetism and Magnetic Materials 293, 702–708.
Meyer, M.H.F., Hartmann, M., Krause, H., Blankenstein, G., Mueller-Chorus, B., Oster, J., Miethe, P., Keusgen, M., 2007. Biosensors and Bioelectronics 22, 973–979.
Mujika, M., Arana, S., Castaño, E., Tijero, M., Vilares, R., Ruano-López, J.M., Cruz, A., Sainz, L., Berganza, J., 2009. Biosensors and Bioelectronics 24, 1253–1258.
Park, H., Kim, D., Yun, K.S., 2010. Sensors and Actuators B (Chemical) 150, 167–173.
Prakash, S.B., Abshire, P., 2007. IEEE Sensors Journal 7, 440–447.

Qureshi, A., Niazi, J.H., Kallempudi, S., Gurbuz, Y., 2010. Biosensors and Bioelectronics 25, 2318–2323.
Raphael, M.P., Christodoulides, J.A., Qadri, S.N., Simpkins, B.S., Byers, J.M., 2010. Nanotechnology 21, 285101.
Richardson, J., Hill, A., Luxton, R., Hawkins, P., 2001. Biosensors and Bioelectronics 16, 1127–1132.
Schotter, J., Kamp, P.B., Becker, A., Pühler, A., Reiss, G., Brückl, H., 2004. Biosensors and Bioelectronics 19, 1149–1156.
Smistrup, K., Kjeldsen, B.G., Reimers, J.L., Dufva, M., Petersen, J., Hansen, M.F., 2005. Lab on a Chip 5, 1315–1319.
Stagni, C., Guiducci, C., Benini, L., Ricco, B., Carrara, S., Paulus, C., Schienle, M., Thewes, R., 2007. IEEE Sensors Journals 7, 577–585.
Sun, N., Liu, Y., Lee, H., Weissleder, R., Ham, D., 2009. IEEE Journal of Solid-State Circuits 44, 1629–1643.
Togawa, K., Sanbonsugi, H., Lapicki, A., Abe, M., Handa, H., Sandhu, A., 2005. IEEE Transactions on Magnetics 41, 3661–3663.
Wang, H., Chen, Y., Hassibi, A., Scherer, A., Hajimiri, A., 2009. IEEE International Solid-State Circuits Conference (ISSCC) Tech. Dig., 438–439.
Wirix-Speetjens, R., Reekmans, G., De Palma, R., Liu, C., Laureyn, W., Borghs, G., 2007. Sensors and Actuators. B (Chemical) 128, 1–4.
Xu, L., Yu, H., Akhras, M.S., Han, S., Osterfeld, S., White, R.L., Pourmand, N., Wang, S.X., 2008. Biosensors and Bioelectronics 24, 99–103.
Yang, S.Y., Lien, K.Y., Huang, K.J., Lei, H.Y., Lee, G.B., 2008. Biosensors and Bioelectronics 24, 855–862.